INSTITUTE OF PHYSICS PUBLISHING NANOTECHNOLOGY
Nanotechnology **17** (2006) 595–599 doi:10.1088/0957-4484/17/2/042

High electron mobility in well ordered and lattice-strained hydrogenated nanocrystalline silicon

X Y Chen, W Z Shen[1], H Chen, R Zhang and Y L He

Laboratory of Condensed Matter Spectroscopy and Opto-Electronic Physics, Department of Physics, Shanghai Jiao Tong University, 1954 Hua Shan Road, Shanghai 200030, People's Republic of China

E-mail: wzshen@sjtu.edu.cn

Received 20 July 2005, in final form 23 November 2005
Published 3 January 2006
Online at stacks.iop.org/Nano/17/595

Abstract
We report on the realization of high electron mobility (over 10^3 cm^2 V^{-1} s^{-1}) in structure-ordered and lattice-strained hydrogenated nanocrystalline silicon (nc-Si:H) due to the decrease of conduction effective mass and phonon scattering. The nc-Si:H thin films were grown on crystalline silicon substrates by plasma-enhanced chemical vapour deposition through the radio-frequency power to properly control the chemical reactions of H atoms with the Si–Si network. The electron mobility and concentration in the nc-Si:H have been extracted with the aid of magnetic-field-dependent Hall effect measurements. X-ray diffraction, Raman, and infrared transmission experiments have been employed to yield information about the lattice strain and structural order in the Si nanocrystals. The room-temperature experimental mobility has been well explained by a generalized Drude transport model unifying both the diffusive and ballistic transport mechanisms.

Hydrogenated nanocrystalline (nc-Si:H) and amorphous (a-Si:H) silicon thin films have been widely used in electronic and optoelectronic devices [1]. With the proposed models of surface diffusion [2], selective etching [3], chemical annealing [4], and ion bombardment effect [5], hydrogen has been demonstrated to play a key role in the nanocrystal nucleation, which determines the electronic and optical properties of these films through the grain size and crystalline fraction. A fundamental understanding of interactions between the hydrogen atoms of plasma and solid silicon matrix is important for optimizing the film structure and properties. By combination of molecular-dynamics simulations and infrared (IR) spectroscopy on a-Si:H films exposed to H_2 (or D_2) plasma, Sriraman *et al* [6] have shown that H-induced crystallization is realized by insertion of H atoms into strained Si–Si bonds through the formation of intermediate bond-centred Si–H–Si configuration and subsequent local structural rearrangements of the broken or perturbed Si–Si bonds.

[1] Author to whom any correspondence should be addressed.

The atomic-scale mechanism facilitates pathways, by controlling the chemical reactions of H atoms with the Si–Si network, to generate large uniform and well ordered Si grains through the H-induced disorder-to-order transformation. Recently, we have successfully established the way to grow nc-Si:H thin films with ordered Si grains and narrow a-Si:H boundaries (about 2–4 atomic spacings in thickness) by radio-frequency (rf) plasma-enhanced chemical vapour deposition (PECVD) [7, 8]. In contrast to the previously reported data of 0.1–10 cm^2 V^{-1} s^{-1} [9, 10], electron mobility of 10^2–10^3 cm^2 V^{-1} s^{-1} has been achieved in nc-Si:H grown on crystalline silicon (c-Si) substrates under optimal growth conditions [11]. Furthermore, the recent strain-engineering technologies have shown quite a success in the mobility enhancement of the strained SiGe materials system [12]. The large strain-dependent change in the electrical properties, known as the piezoresistance effect [13], originates from both the effective mass change of individual valleys and the intervalley carrier transfer.

The combination processes of the H insertion by bond breaking, bond reformation, and network rearrangement during the nanocrystal nucleation open the great possibility of growing lattice-strained Si grains in the nc-Si:H thin films. In fact, strained Si lattices have been demonstrated in the nc-Si:H grains before [14]. In PECVD, the rf power has been found to have a large effect on the incorporation and interaction between H atoms and the Si–Si network, which determines the growth of Si grains (i.e. the average grain size, lattice strain, and structural order). This paper reports on the realization of well ordered and lattice-strained nc-Si:H thin films with high electron mobility (over 10^3 cm^2 V^{-1} s^{-1}) by properly controlling the growth of Si nanocrystals through the rf power, implicating high-mobility electronic device application of nc-Si:H with the PECVD's advantages of low-cost and large-area deposition at low temperature.

The phosphorus-doped nc-Si:H thin films with thickness of $\sim$1.0–4.5 μm were prepared in an rf (13.56 MHz) capacitive coupled PECVD system from silane (SiH_4) and H_2 on high-purity c-Si substrates ($<10^{15}$ cm^{-3}) at a temperature of 250 °C and chamber pressure of 0.7–1.0 Torr. The percentage content of silane ($SiH_4/SiH_4 + H_2$) is about 1.0%. Two sets of nc-Si:H samples were employed in the present investigation. The first set (R series) samples were fabricated with the rf power varying from 90 to 30 W (90 W, R1; 75 W, R2; 45 W, R3; 30 W, R4) at a fixed phosphine doping ratio (PH_3/SiH_4) of 0.8%, while the second set (D series) with the phosphine doping ratio of 0–10.0% (0%, D1; 0.5%, D2; 1.0%, D3; 5.0%, D4; 10.0%, D5) at a fixed rf power of 60 W.

The structure of these nc-Si:H thin films has been characterized by x-ray diffraction (XRD), Raman, and IR transmission measurements, which were performed on a Bruker-axs D8Advance instrument in the standard θ–2θ configuration, a Jobin Yvon LabRAM HR800 UV micro-Raman system in backscattering configuration under a 514.5 nm laser with a penetration depth $\sim$ 300 nm in nc-Si:H, and a Nicolet Nexus 870 Fourier transform infrared spectrometer, respectively. For the transport measurements, considering the fact that there are three planar conducting layers in the nc-Si:H/c-Si heterostructures: nc-Si:H thin film, c-Si substrate, and their interfacial two-dimensional electron gas [8, 11], we have employed the magnetic-field-dependent Hall effect measurements with a Van der Pauw configuration under an Oxford Instruments superconductive magnet (magnetic field up to 15 T), followed by the mobility spectrum analysis [15] technique. The details for extracting the individual transport parameters (carrier mobility, concentration, and type) have been described elsewhere [8, 11].

Figure 1 shows the yielded room-temperature experimental (scattered points) electron mobility μ as a function of electron concentration n in the two sets of nc-Si:H samples, together with the error limits due to the uncertainty in the mobility spectrum analyses. We note that the variation of electron concentration with the rf power is trivial in the R set samples, since these samples were fabricated under the same phosphine doping ratio of 0.8%. In contrast, we can observe a large difference in the resultant electron mobility. For the D set samples, it is expected that the electron concentration changes significantly with the phosphine doping ratio, and the electron mobility is found to decrease monotonically with the increase of electron concentration.

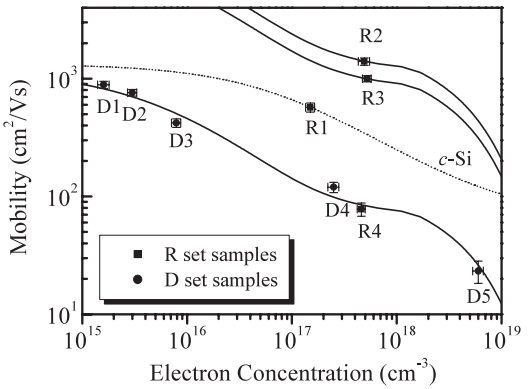

Figure 1. Room-temperature mobility versus electron concentration from the magnetic-field-dependent Hall effect measurements in the two sets of nc-Si:H thin films grown by PECVD. Samples R1–R4 are grown under the rf power of 90, 75, 45, and 30 W at a fixed phosphine doping ratio of 0.8%, while samples D1–D5 with the phosphine doping ratio of 0, 0.5, 1.0, 5.0, and 10.0% at a fixed rf power of 60 W. Experimental data, scattered points; theoretical results from the generalized Drude transport model, solid curves. The experimental bulk c-Si mobility in [23] has been shown as the dotted curve.

We start with the structural information for the detailed theoretical explanation of the above experimental mobility. Figures 2(a) and (b) present the experimental XRD results (dotted curves) for the two sets of nc-Si:H samples. The dashed lines indicate the positions of the (111), (220), and (311) diffraction peaks in the conventional coarse-grained polycrystalline Si. The good quality of the Si nanocrystals is evidenced by the relatively sharp and symmetric (111) diffraction peak, together with two broad (220) and (311) structures (please note the different x-axis scales there). It is well known that the position and broadening of the diffraction peaks reflect the lattice constant and grain size in the nanocrystals, which can be obtained through the Bragg diffraction equation and Scherrer formula, respectively [14, 16]. From figure 2, we can observe a large deviation of the diffraction peak positions from the dashed lines, especially for the (111) peak, in the R set samples, in contrast to the almost coincidence in the D set case. These results indicate that there is lattice strain in the Si nanocrystals of R set samples, while it is nearly relaxed in the Si grains of D set ones. The lattice strain can be shown by the relative lattice constant difference between the nanocrystal and bulk c-Si. Through Lorentzian fitting (solid curves) of the (111) diffraction peak [16], we have displayed in figures 2(c) and (d) the average lattice strain (the positive (negative) value reflects the tensile (compressive) case) and grain size in these nc-Si:H thin films. The split of the (111) diffraction peak, especially in samples R1 and R3, implicates a distribution of the (111) lattice plane separations, resulting in a relatively large uncertainty for determining the lattice strain and grain size in R1 and R3 (see the error bars in figures 2(c) and (d)). Vepřek *et al* [14] have also observed a similar phenomenon in the nc-Si:H thin films. It is clear that the rf power has played a key role in both the average lattice strain and grain size during the growth of Si grains in PECVD.

Figure 3 shows the room-temperature IR transmission spectra of these nc-Si:H samples, where the substrate

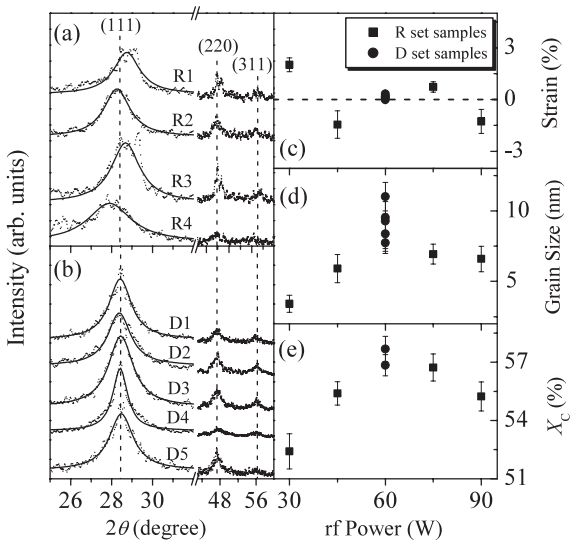

Figure 2. X-ray diffraction patterns for the (a) R set and (b) D set nc-Si:H thin films. The resultant average (c) lattice strain, (d) grain size from the Lorentz fitting of the (111) diffraction peak, and (e) crystalline fraction X_C from the Raman measurements.

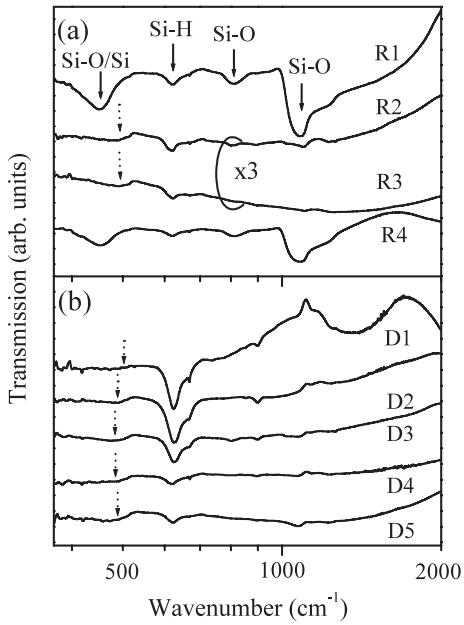

Figure 3. Room-temperature IR transmission spectra for the two sets of nc-Si:H thin film samples. The spectra of samples R2 and R3 have been multiplied by a factor of three for clarity.

absorption contribution has been removed through dividing the sample spectra by those of bare c-Si substrates. Firstly, we can clearly observe the Si–H wagging mode at ∼620–630 cm^{-1} [17] in all samples. This indicates that the H atoms saturate the dangling bonds there, and cause the formation of Si nanocrystals, as revealed in the XRD results of figure 2. Secondly, as we know, except for perfectly ordered structures, the crystal moment and symmetry selection rules will be relaxed, resulting in dipole-allowed photon absorption with creation of a phonon. This process in the nc-Si:H will result in the absorption of a transverse optical (TO)-like stretching mode of the Si–Si bonds at ∼450–510 cm^{-1} [18]. In contrast to the strong Si–Si vibrations at ∼455 cm^{-1} in the two excessively high (R1) and low (R4) rf power samples, only weak absorption (dashed arrows) at ∼490–510 cm^{-1} has been observed in the other nc-Si:H samples. The blueshift of the TO-like mode reflects that the structure of the nc-Si:H becomes very ordered, which has been demonstrated in extensive Raman experiments [19]. In fact, the weak TO-like Si–Si IR absorption in the ordered nc-Si:H thin films is due to the decrease of the disorder-induced lattice charge. Thirdly, clear Si–O absorption bands have been observed in the two excessively high (R1) and low (R4) rf power samples (figure 3(a)), indicating relatively high concentration of O impurity. The absorption bands at ∼810 and ∼1100 cm^{-1} correspond well to the characteristic Si–O bending and stretching modes [20], respectively. Therefore, the Si–O rocking mode at ∼450 cm^{-1} may also contribute to the strong absorption peak at ∼455 cm^{-1}, in addition to the contribution of the Si–Si bonds. The excess oxidation appears to be associated with an increase in the defect density, resulting in disordered structures there [21].

The increase of rf power in the PECVD helps to enhance the diffusion length of the precursors and to aid in speeding the growth rate of the grains [19], resulting in the increase of ion numbers and kinetic energy, which in turn increases the average grain size. However, excessive etching action of H atoms at high rf powers will decrease the growth rate of the grains, limiting the average grain size. This explains the observed maximum average grain size in the nc-Si:H samples grown under the rf power of 60 W (figure 2(d)). As is well known, the lattice strain in the nanocrystals is energetically favourable for minimizing the interfacial energy due to a large density of defects and dislocations at the grains' interfaces [14]. The increase of grain size would relax its internal lattice strain, leading to disappearance of strain in the large-size grains such as the microcrystalline Si thin films. Therefore, the lattice strain in the Si nanocrystals grown under the rf power of 60 W (the D set samples) is much weaker (∼0.01–0.3%) than that of the R set ones (∼1–2%) with relatively smaller grain sizes (see figure 2(c)). In addition, it is expected from the above growth mechanism (i.e. the double effects of etching action of H atoms [19]) that too high or too low rf power will not favour for the fabrication of structure-ordered nc-Si:H thin films (figure 3(a)), exhibiting the reduction of the crystalline fraction X_C in the Raman measurements (figure 2(e)). For the determination of X_C, the Raman spectra were decomposed into three Gaussian phonon bands with peaks at 480, 510, and ∼520 cm^{-1}. X_C and its error limit were then given by the ratio of the integrated intensity of the Gaussian bands centred at 510 and ∼520 cm^{-1} to the total integrated intensity of the three bands [4] and the uncertainty in the fitting procedure. The above arguments clearly demonstrate the large effect of the rf power on the incorporation and interaction between the H atoms and Si–Si network [6], which determines the growth of Si grains (i.e., the average grain size, lattice strain, and structural order).

In the nc-Si:H thin films, the trapping states at the a-Si:H boundaries would cause the depletion of electrons in Si grains, resulting in the formation of an electronic band structure with

three-dimensional potential barrier. The depletion region in the grains changes with the doping concentration, which in turn results in the variation of the electronic band structure (i.e. barrier height and width). The electron mobility of nc-Si:H thin films can be described by a generalized Drude transport model within the diffusive and ballistic transport mechanisms: $\mu = \gamma\mu_e$ [22]. In our nc-Si:H samples, high resolution transmission electron microscopy has revealed very narrow a-Si:H boundaries (about 2–4 atomic spacings in thickness, much less than the average grain size) [7]. For the case of extremely narrow a-Si:H boundaries, the diffusive mobility μ_e in nc-Si:H can be considered the same as in c-Si. The factor γ reflects the boundary scattering in the ballistic transport of carriers through the barriers, which is strongly related to doping concentration, electron mean free path, and trapping states at the a-Si:H boundaries.

For the strain-relaxed D set samples, it is clear, from figure 1, that their mobility is lower than that of unstrained bulk c-Si (dotted curve by $\mu_e = 65 + 1265/[1 + (n/8.5 \times 10^{16})^{0.72}]$ cm^2 V^{-1} s^{-1} from [23]) at the same concentration due to the formation of electron barriers at the grain boundaries. The factor γ is determined by the periodic parabolic energy band, which can be obtained from the Poisson function of potential energy in the depletion region under different doping concentrations [22]. The solid curves in figure 1 are the theoretical results from the generalized Drude transport model, which can well explain the experimental observation for the D set samples. This result clearly demonstrates the control of the electronic band structures by shallow impurity phosphorus doping in Si nanocrystals. In addition, the generalized Drude transport model can also expect the Mott transition from the extended state conductance to bandtail state conductance in nc-Si:H with the decrease of temperature.

It is interesting to note that we can achieve very high electron mobility in the R set nc-Si:H samples of figure 1, especially over 10^3 cm^2 V^{-1} s^{-1} in R2 and R3. Such a high mobility is not due to the disappearance of the a-Si:H boundaries, since we have demonstrated clearly the barrier scattering in R2 by the extended state–bandtail state Mott transition [11]. From the structural information of figures 2 and 3, we understand that these two special samples consist of well ordered and lattice-strained Si grains. Our high-resolution transmission electron microscopy has also revealed the well ordered nc-Si microstructure [11]. The study for bulk c-Si under external stress [13] has demonstrated the tunable carrier mobility through the effective mass and phonon scattering, and the recent strain-engineering technologies have shown fair success in the mobility enhancement of strained SiGe materials system [12]. We therefore attribute the high mobility to the strain effect in the Si nanocrystals.

At room temperature, the phonon scattering dominates the electron transport process in the extended conductance state due to the low potential barrier (∼10 meV) in the R set nc-Si:H samples. As we know, the phonon scattering time τ in nonpolar semiconductor Si has the relationship with effective mass m^* and temperature T of $\tau \propto (m^*)^{-3/2}T^{-3/2}$ [24]. The diffusive mobility μ_e^{st} in the strained nc-Si:H from the phonon scattering can thus be simplified as $\mu_e^{st} = \mu_e(m_{st}^*/m_0^*)^{-5/2}$, with m_{st}^* and m_0^* the conductivity effective masses of electrons in the strained and unstrained Si grains, respectively. In the nc-Si:H thin films, the ballistic transport factor γ will also be modified by the conductivity effective mass change. The theoretical mobility $\mu^{st} = \gamma\mu_e^{st}$ as a function of electron concentration by the generalized Drude transport model with $m_{st}^* = 0.32m_0^*$ and $0.37m_0^*$ (solid curves in figure 1) can well explain the experimental data for the two special samples R2 and R3, respectively. The observed high mobility is therefore due to the strain-induced reduction of conductivity effective mass, which reflects the decrease of both the electron effective mass and phonon scattering in the nc-Si:H. In fact, in the highly ordered structure of c-Si thin films under 1% biaxial tensile strain in the [001] direction, the electron mobility can be up to about 3.5×10^3 cm^2 V^{-1} s^{-1} [12], which is much higher than that of $\sim 1.0 \times 10^3$ cm^2 V^{-1} s^{-1} in the present strained nc-Si:H samples (R2 and R3) due to the boundary scattering. In addition, the 1% anisotropic compressive strain in the bulk c-Si could also increase the conductivity by over tenfold [25]. As a result, the observed high electron mobility in the strained nc-Si:H samples (figure 1) is out of expectation, but reasonable.

Finally, it should be noted that, in addition to the lattice strain, well ordered structure is another necessary condition for achieving high mobility in nc-Si:H thin films. According to Anderson localization theory [26], the carriers will be localized in disordered structures, which cause the decrease of the carrier mobility. Samples R1 and R4 have relatively disordered structures (figure 3(a)) and low crystalline fraction (figure 2(e)) due to the too high/low rf power during the PECVD fabrication. We therefore observe the rapid decrease of the electron mobility there (figure 1), though they have very large lattice strain (figure 2(c)). As a result, it is clear that high electron mobility can only be realized in both well ordered and lattice-strained PECVD nc-Si:H thin films, where the rf power has played a key role in the growth of Si grains through controlling the chemical reactions of H atoms with Si–Si bonds.

In summary, we have carried out a detailed transport and structural investigation on nc-Si:H thin films grown on c-Si substrates by PECVD with different rf powers and doping concentrations. The experimental mobility has been well explained by a generalized Drude transport model based on the diffusive and ballistic transport mechanisms. In addition to the expected electron mobility with different doping levels (due to the variation of the electronic band structures) in ordered and strain-relaxed nc-Si:H samples, we have realized high-mobility (over 10^3 cm^2 V^{-1} s^{-1}) Si nanocrystals through adjusting the rf power in PECVD to optimize the incorporation and interaction of H atoms and Si–Si network for the formation of both structure-ordered and lattice-strained nc-Si:H thin films. The employment of strained Si grains in nc-Si:H (with small electron effective mass and reduced phonon scattering) provides an effective way to improve the electron mobility for the high-speed/high-frequency electronic device application of nc-Si:H.

Acknowledgments

This work was supported in part by the Natural Science Foundation of China under contract Nos 10125416 and 60576067, and the Shanghai municipal major basic research project 03DJ14003.

References

[1] Shah A, Torres P, Tscharner R, Wyrsch N and Keppner H 1999 *Science* **285** 692
[2] Nomoto K, Urano Y, Guizot J L, Ganguly G and Matsuda A 1990 *Japan. J. Appl. Phys.* 2 **29** L1372
[3] Layadi N, Roca i Cabarrocas P, Drevillon B and Solomon I 1995 *Phys. Rev.* B **52** 5136
[4] Kasier I, Nickel N H, Fuhs W and Pilz W 1998 *Phys. Rev.* B **58** R1718
[5] Kalache B, Kosarev A I, Vanderhaghen R and Roca i Cabarrocas P 2003 *J. Appl. Phys.* **93** 1262
[6] Sriraman S, Agarwal S, Aydil E S and Maroudas D 2002 *Nature* **418** 62
[7] He Y L, Hu G Y, Yu M B, Liu M, Wang J L and Xu G Y 1999 *Phys. Rev.* B **59** 15352
[8] Chen X Y and Shen W Z 2004 *Appl. Phys. Lett.* **85** 287
[9] Nasuno Y, Kondo M and Matsuda A 2001 *Appl. Phys. Lett.* **78** 2330
[10] Cheng I C and Wagner S 2002 *Appl. Phys. Lett.* **80** 440
[11] Chen X Y, Shen W Z and He Y L 2005 *J. Appl. Phys.* **97** 024305
[12] Lee M L, Fitzgerald E A, Bulsara M T, Currie M T and Lochtefeld A 2005 *J. Appl. Phys.* **97** 011101
Fischetti M V and Laux S E 1996 *J. Appl. Phys.* **80** 2234
[13] Smith C S 1954 *Phys. Rev.* **94** 42
Kanda Y and Suzuki K 1991 *Phys. Rev.* B **43** 6754
[14] Vepřek S, Sarott F-A and Iqbal Z 1987 *Phys. Rev.* B **36** 3344
[15] Beck W A and Anderson J R 1987 *J. Appl. Phys.* **62** 541
[16] Fitzsimmons M R, Eastman J A, Müller-Stach M and Wallner G 1991 *Phys. Rev.* B **44** 2452
[17] Brodsky M H, Cardona M and Cuomo J J 1977 *Phys. Rev.* B **16** 3356
[18] Shen S C, Fang C J, Cardona M and Genzel L 1980 *Phys. Rev.* B **22** 2913
[19] Saha S C, Barus A K and Ray S 1993 *J. Appl. Phys.* **74** 5561
[20] Tsu D V, Lucovsky G and Davidson B N 1989 *Phys. Rev.* B **40** 1795
[21] Lucovsky G, Nemanich R J and Knights J C 1979 *Phys. Rev.* B **19** 2064
[22] Weis T, Lipperheide R, Wille U and Brehme S 2002 *J. Appl. Phys.* **92** 1411
Lipperheide R, Weis T and Wille U 2001 *J. Phys.: Condens. Matter* **13** 3347
Chen X Y and Shen W Z 2005 *Phys. Rev.* B **72** 035309
[23] Caughey D M and Thomas R E 1967 *Proc. IEEE* **55** 2192
[24] Sze S M 1981 *Physics of Semiconductor Devices* 2nd edn (New York: Wiley) chapter 1
[25] Seeger K 1973 *Semiconductor Physics* (Wien: Springer)
[26] Lee P A and Ramakrishnan T V 1985 *Rev. Mod. Phys.* **57** 287